SUPPLEMENTARY INFORMATION:

1. INTERIOR DIFFERENTIATION AND METHANE CLATHRATE STABILITY

1.1 Density of materials composing Titan's interior:

The differentiation of Titan is mainly driven by the density differences among materials composing the interior. In order to quantify this effect, we compute the density ρ of different materials as a function of pressure from the experimentally determined bulk modulus following Croft *et al.* (1988):

$$\rho = \rho_0(T_0, P_0) \times \left[\frac{K_0^{'} P}{K_0} + 1 \right]^{1/K_0^{'}} \qquad (1),$$

where ρ_0 is the density at the reference pressure P_0, K_0 is the isothermal bulk modulus and $K_0^{'}$ is the pressure derivative of the bulk modulus. Table 1 summarizes the parameter values used for each material. For the ammonia-water system, those parameters are computed following Croft *et al*. (1988). For methane hydrate and ammonia hydrate, the density at reference pressure is calculated from the mean molecular volume V_{mol} and the molecular mixing ratio of water given by Loveday *et al.* (2001) and Loveday and Nelmes (2003). Densities as a function of pressure are displayed on Figure 1. For the liquid ammonia-water solution, two different ammonia concentration values are considered: 0% and 15%. Whatever the pressure values methane hydrate is the least dense material, being equal in density to water ice at low pressure (P<0.2GPa). Even for 15% ammonia-water liquid, methane clathrate is still 2% less dense. The computed value corresponds to the maximum value because full cage occupancies are assumed. In practice, small cage filling has been reported to be significantly lower than (but still of order) 1 at low pressure (Klapproth *et al.* 2003). For small and large cage filling values of 0.7 and 0.9 respectively, the methane hydrate density is equal to 900 $kg.m^{-3}$, 2% less than water ice. Due to its very low density (Fig. 1), methane clathrate irremediably rises toward the surface, forming a methane clathrate-enriched layer. The accumulation of methane clathrate in the outer layer depends on the amount of methane initially trapped or produced within the interior and the rate of its release.

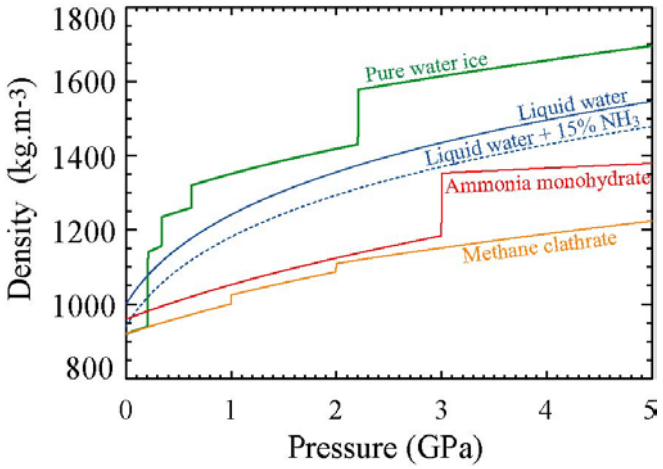

Figure 1: *Density of different materials composing Titan's interior: pure water ice in green, liquid water with an ammonia mass fraction of 0 and 15% in blue, ammonia monohydrate in red and methane clathrate hydrate in orange. Methane hydrate is the least dense material for pressure over 200 MPa and has a density similar to low pressure phase ice (ice I) below 200 MPa.*

Table 1: *Parameters to compute the density as a function of pressure*

	Reference pressure P_0 (GPa)	***Density at P_0 ρ_0 (kg.m^{-3})***	***Isothermal bulk modulus K_0 (GPa)***	***K'_0***	***Reference***
Ammonia-water	10^{-4}	Computed at T=300K[a]	Computed at T=300K[a]	Computed at T=300K[a]	Croft *et al.* 1988
Ice					
Ice I	10^{-4}	920	9.2	5.5	Sotin *et al.* 1998
Ice III	0.207	1140	8.5	5.7	Sotin *et al.* 1998
Ice V	0.34	1235	13.2	5.2	Sotin *et al.* 1998
Ice VI	0.62	1320	14.9	6.6	Sotin *et al.* 1998
Ice VIII	2.21	1460	24	4.15	Hemley *et al*. 1987
Methane Hydrate					
MHI	10^{-4}	920	~10[b]	4	Loveday *et al*. 2001
MHII	1	1025	~15[b]	4	Loveday *et al*. 2001
MHIII	2	1120	~25[b]	4	Loveday *et al*. 2001
Ammonia MonoHydrate					
AMHI	10^{-4}	960	8.9	4.2	Loveday and Nelmes 2003
AMHIV	3	1355	~100[b]	4	Loveday and Nelmes 2003

[a] We follow the method presented in Croft et al. (1988) to compute the reference density ρ_0, the isothermal bulk modulus K_0 and its derivative K'_0 of the ammonia-water solutions.

[b] Isothermal bulk modulus estimated from the data provided in Loveday *et al.* (2001) and Loveday and Nelmes (2003).

1.2 Stability curves of methane clathrate in presence of ammonia:

To parameterize the stability curve of methane clathrate hydrate in water solutions, we have performed a polynomial fit of the available experimental data over a wide range of pressure (Dyadin et al. 1997, Sloan 1998):

$$T_d^0 = 264.395 + 21.105 \times \log_{10} P - 0.0424805 \times (\log_{10} P)^2, \qquad (2)$$

with T_d^0 the dissociation temperature in the binary water-methane system in Kelvins, P the pressure in MPa. To take into account the well-know inhibiting effects of ammonia on methane clathrate (Sloan 1998), we use the parameterization proposed for salt water solutions (Dickens and Quinby-Hunt 1997) using the data on the binary ammonia-water system (Grasset and Pargamin 2005):

$$T_d^{xNH3} = \left\{ \frac{1}{T_d^0} - \frac{n\Delta H_f}{\Delta H_d} \left[\frac{1}{T_f^0} - \frac{1}{T_f^{xNH3}} \right] \right\}^{-1} \qquad (2),$$

where T_f^0 and $T_f^{x_{NH_3}}$ are the fusion temperature of ice for the pure water system and ammonia-water system, respectively, computed using the method described by Grasset and Pargamin (2005). ΔH_d is the enthalpy of dissociation for methane clathrate to liquid water and methane gas, n is the hydration number ($\Delta H_d / nR$ is estimated to 1090 K). ΔH_f is the enthalpy of fusion for pure water to ice (6008 J.mol^{-1} at 273.2 K, Dickens and Quinby-Hunt 1997).

As Fig. 2 illustrates, ammonia reduces the stability of methane clathrate at almost the same extent that it decreases the crystallization point of ammonia-water solutions. The net effect is small and is equivalent to a change in the steady-state temperature of the interior ocean. Therefore any methane clathrate released during the overturn that formed a discrete rock core would ascend to the top of the outer liquid layer without being dissociated. Moreover, even if heating in the proto-core were to have induced local dissociation of methane clathrate during core formation (i.e. T_{core}>400 K), methane should have been re-enclathrated before reaching the surface due to the high stability of clathrate within the temperature-pressure regime of the ammonia-water ocean (Grasset and Pargamin 2005).

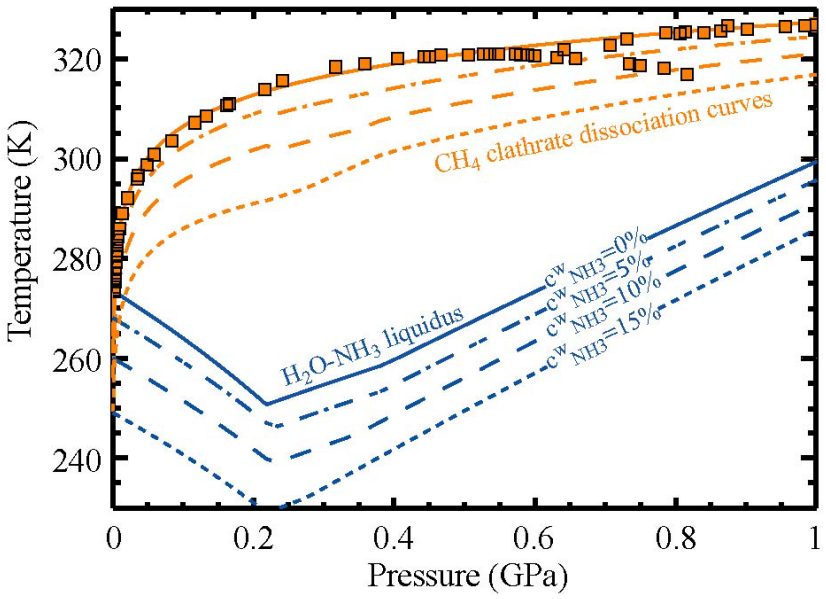

Figure 2: *Stability curve of methane clathrate hydrate in orange compared to the melting curve of ice in blue for different ammonia mass fractions in the liquid phase. Orange squares represent experimental data given by Dyadin et al. (1997). Curves with similar line styles correspond to the same ammonia fraction.*

2. LONG TERM EVOLUTION MODELS OF TITANS INTERIOR

The model we used in this study is a modified version of the model used and described in Tobie *et al.* (2005a). As in the former version, the cooling and crystallisation of Titan's interior, including ammonia, are computed simultaneously with tidal dissipation and orbital evolution. Additional developments in the present study consist of the incorporation of methane clathrate hydrate within the outer layer above the internal ocean. Accordingly, the numerical scheme has been modified to take into account the particular thermo-mechanical properties of methane clathrate hydrate, which are very different from water ice. The main effect of methane hydrate is to modify the heat transfer through, and equilibrium temperature at the base of, the outer icy layer. The evolution is computed using a fully implicit numerical scheme and the timestep is fixed at a value of 10^5 years. At each time step, heat transfer through the outer layer and tidal dissipation within the interior are computed, a new value of radius for each interface is derived, and the eccentricity decay is calculated with respect to global tidal dissipation. Each element of the models is described further below.

2.1 Evolution of the silicate core

A fully differentiated structure is unlikely to exist just after Titan's accretion. More probably, a mixed ice-rock core may exist below a silicate mantle and an outer H_2O layer

once its accretion is achieved (Kirk and Stevenson 1987, Lunine and Stevenson 1987). The complete segregation of ice and rock mixture within the core occurs roughly 500 million years after accretion (Lunine and Stevenson 1987). We start the evolution of Titan at t=0.5 Ga once the core overturn is achieved and once the rapidly declining rate of meteoritic bombardment can be safely neglected.

We consider three different silicate compositions, having different density ρ_{sil} and initial radiogenic heating H_0, and corresponding to different core size R_{sil} and global mass fraction x_{sil} in order to fit Titan's measured mean density:

1- Hydrated silicate : ρ_{sil}=3000 kg.m^{-3}, H_0=3.10^{-11} W.kg^{-1}, R_{sil}=1900 km, x_{sil}=0.64.

2-Silicate similar to Earth's upper mantle: ρ_{sil}=3300 kg.m^{-3}. H_0= 4.10^{-11} W.kg^{-1}, R_{sil}=1800 km, x_{sil}=0.6.

3- Anhydrous silicate: ρ_{sil}=4000 kg.m^{-3}, H_0= 5.10^{-11} W.kg^{-1}, R_{sil}=1625 km, x_{sil}=0.53.

Heat flow coming out of the silicate core is determined by both the amount of radiogenic elements and the efficiency of heat transfer. Tidal dissipation within the silicate interior is very low and can be neglected (Sohl *et al.* 2003, Tobie *et al.* 2005b). The early thermal evolution of a homogeneous chondritic core is characterized by a temperature increase controlled by diffusive heating. Depending on the composition of the silicates there, we assume the core becomes unstable against thermal convection for internal temperature of 1400K, 1500K, 1600K, corresponding to core composition 1, 2 and 3, respectively. Indeed, silicate hydration is known to lower the silicate viscosity (e.g. Karato and Wu 1993), and then to make the silicate core unstable at lower temperature. Once the core start convecting at 1.8, 2.0 and 2.6 Ga for core composition 1, 2 and 3 respectively, an equilibrium state is reached only few hundred million years after the onset of convection (Tobie 2003). Then the global heat power coming out of the silicate core includes contributions from both radiogenic decay and secular cooling, so that after initiation of convection the interior expels more heat than provided by radiogenic decay. We have tested the effect of silicate thermal conductivity and heat capacity over a reasonable range of values [k_{sil}=3-5 W.m^{-1}.K^{-1}, c_{sil}=800-1200 J.kg^{-1}.K^{-1}]. Varying the heat capacity changes the time at which the critical core temperature is reached and therefore of the onset of convection: in scenario 1, 2.0 <t_{onset}< 3.1 Ga; in scenario 2, 1.6 <t_{onset}< 2.5 Ga, in scenario 3, 1.5 <t_{onset}< 2.1Ga. Variations of the thermal conductivity change the heat flux during the diffusive stage by 10-15% and only slightly the onset time of convection. Even though uncertainties in the heat capacity values as well as the possible formation of an iron core, especially in scenario 3, may change the time of convection onset, the change is not sufficient to alter qualitatively the overall evolution of the silicate core. We believe that the three examples represented on Fig. 1 in the letter give a reasonable range of possible core evolutions.

2.2 Tidal dissipation and orbit evolution

Body tide dissipation is calculated by integrating the equations of motions and Poisson's equation from the centre of the satellite to its surface, and by imposing the tide-generating potential induced by Saturn at the surface (Tobie *et al.* 2005b). Assuming a compressible Maxwell rheology, the viscoelastic properties of each layer are defined from the values of the elastic S- and P-wave velocities, V_S and V_P respectively, and the effective Newtonian viscosity η(see Table 2). The elastic shear and bulk moduli, μ_E and K_E respectively, are related to the S- and P- wave velocities (listed in Table 2 for each internal layer) by the following relationship: $\mu_E = \rho V_S^2$, and $K_E = \rho V_P^2 - 4/3\mu_E$. Temperature dependent viscosity of ice Ih and methane clathrate is evaluated from the homologous temperature T/T_m^0 (e.g., Kirk and Stevenson 1987) and assuming that methane clathrate viscosity is 50 times higher than water ice at the same temperature (Durham *et al.* 2003):

$$\eta(T, x_{MH}) = \left[1 - x_{MH} + x_{MH}/50\right]^{-1} \eta_{m,0} \exp\left(\frac{E_a}{RT_m^0}\left[T_m^0/T - 1\right]\right), \qquad (3),$$

where T_m^0 is the melting temperature of pure water ice Ih, $\eta_{m,0}$ is the viscosity of pure ice Ih at the melting point, E_a is the activation energy (see Table 2), and x_{MH} is the methane hydrate mass fraction. The same formulation is used for the temperature dependence of high-pressure ices, and the homologous temperature T/T_m^0 is assumed constant through the high-pressure ice layer. For the numerical computation of Titan's radial functions (see Tobie *et al.* 2005b), the outer layer is divided into five sublayers in the conductive part and ten sublayers in the convective part, in the liquid layer and in the high-pressure layer. The radial functions of the satellite are not re-computed at each time step, but only when the cumulative radius variations at all interfaces, as defined in Table 2, exceed 2 km.

The global dissipation rate *dE/dt* is computed by integrating the specific dissipation rate H_{tide} calculated in each layer of the model. From the global tidal dissipation rate *dE/dt*, the temporal evolution of Titan's orbital parameters is assessed using the conservation of angular momentum under the assumption of orbital synchronicity. Peale (1977) showed that even if Titan spun rapidly after its accretion, tides raised on the satellite by Saturn must have slowed down its rotation toward synchronicity before core overturn was achieved (t<0.5Ga). Then, the loss of Titan's orbital energy appears as a reduction in orbital eccentricity (Sears 1995), and the change in eccentricity due to tidal dissipation is given by (Sohl *et al.* 1995):

$$\frac{de}{dt}\frac{e}{1-e^2} = \frac{-a}{GM_S M_T}\frac{dE}{dt}, \qquad (4)$$

where M_S and M_T are the mass of Saturn and Titan, respectively, e is the eccentricity, a is the semi-major axis of the orbit. In addition, the conservation of orbital angular momentum implies: $a(1-e^2)=a_c(1-e_c^2)=a_0(1-e_0^2)$. The indices *0* and *c* refer to the initial and current state, respectively. This formulation does not take into account the tidal expansion of Titan's orbit due to dissipation of tides raised by Titan on Saturn. However, for realistic values of dissipation factors, Q_T and Q_S, within Titan and Saturn, (Q_T<500

(this study) and Q_S>10^4 (Peale 1999)), the effect of dissipation within Saturn corresponds to less than 2% of the effect of dissipation within Titan on the eccentricity variation, and therefore can be safely neglected.

2.3 Heat transfer through the outer layer

Heat can be transferred either by thermal diffusion or convection, depending on layer thickness and on its composition. Viscosity and thermal diffusivity as a function of depth within the layer are assumed to be dependent on composition (ice and methane clathrate) and temperature. Only the ice fraction is temperature-dependent. For the methane fraction, no temperature dependence of thermal conductivity k_{MH} and of heat capacity c_{MH} are seen in the available experimental data. Therefore, we assume the thermal conductivity and heat capacity of methane clathrate to be constant. The thermal conductivity $k_{I/MH}$ and heat capacity $c_{I/MH}$ of the mixture are expressed as:

$$k_{I/MH} = x_{MH} k_{MH} + (1 - x_{MH}) \times (k_1 / T + k_2),$$

$$c_{I/MH} = x_{MH} c_{MH} + (1 - x_{MH}) \times (c_1 T + c_2),$$

where the indices I, MH, I/MH refer to ice I, methane hydrate and the mixture, respectively. x_{MH} is the mass fraction of methane hydrate. See table 2 for constant values.

We have developed a new numerical scheme to parameterize thermal convection within a layer heated both from within and from below. Energy from within and from below are provided by tidal dissipation within the layer and by radiogenic heating in the core plus tidal dissipation within the high pressure ice layer, respectively. As long as the outer layer is stable against thermal convection, the temperature profile is computed by solving the diffusion equation including tidal dissipation and temperature- and composition-dependent diffusivity with a Crank-Nicholson scheme. One hundred sublayers are used to resolve the temperature profile in the diffusive layer. The whole layer (methane clathrate sublayer + ice I sublayer) becomes unstable against convection when the Rayleigh number associated with the ice I layer, defined as $Ra=\alpha_I \rho_I g \Delta T b^3 / \kappa_I \eta_I$ exceeds 1100 (Stengel et al. 1982). Then the outer layer is divided into two sublayers: an upper conductive layer made of methane clathrate and a lower isoviscous convective layer made of a mixture of methane clathrate and ice I. Due to the low thermal conductivity of methane clathrate, the temperature gradient is very steep within the conductive lid and the conductive lid is about 2-3 km thin just after the onset of convection. As previously, the temperature profile in the conductive lid is computed by solving the diffusion equation including tidal dissipation and temperature- and composition-dependent diffusivity with a Crank-Nicholson scheme. In the convective sublayer, the homologous T/T_m is assumed to be constant. The evolution of the convective sublayer is determined through scaling laws relating heat fluxes and temperature differences across the thermal boundary layers

(Grasset and Parmentier 1998, Dumoulin *et al.* 1999, Deschamps and Sotin 2001, Tobie 2003). In order to self-consistently include heating from within and from below, those scaling laws are constrained from numerical experiments of thermal convection including viscosity-dependent tidal heating (Tobie *et al.* 2003, Tobie 2003). Heat fluxes at the base and at the top of both convective and conductive ice Ih sublayers, as well as internal heating due to tidal dissipation in the convective sublayer are used to compute the temperature evolution of the well-mixed convective sublayer and the evolution of the thickness of the overlying conductive lid. For this purpose, we use the formulation proposed by Schubert and Spohn (1990).

2.4 Evolution of the liquid layer and clathrate dissociation

The evolution of the liquid layer depends on the rate of methane clathrate dissociation and on the rate of ocean crystallization. Thickness and temperature variations of the liquid water layer are determined using heat flux values obtained at the base of the outer layer, R_{IO}, and at the top of the high-pressure ice layer, R_{OHP}, (i.e. heat flow from the silicate core – due mainly to the radiogenic decay of isotopic elements - plus tidal dissipation in the high-pressure ice layer). We use the numerical scheme proposed by Grasset and Sotin (1996) for the evolution of the liquid water layer, which we have modified to take into account methane clathrate dissociation. Depending on the composition (ice I or methane clathrate) at the base of the outer layer, the interface temperature is controlled by the methane clathrate dissociation temperature (see "Stability curves of methane clathrate in presence of ammonia"**)** or the NH_3-H_2O liquidus. The temperature evolution of each solid/liquid interface, T_{IO} and T_{OHP}, during the ocean crystallization or during the clathrate dissociation, and the variation of ammonia concentration $C^{w}_{NH3}=M_{NH3}/M_{liquid}$ in the liquid layer (where M_{NH3} and M_{liquid} are the mass of ammonia and the mass of the liquid layer respectively), are calculated accurately using a new algorithm describing the liquidus in the H_2O-NH_3 system (Grasset and Pargamin 2005). When the pressure-dependent dissociation temperature of methane clathrate is reached, we set the ocean/clathrate interface temperature, T_{IO}, to be the dissociation temperature, T_d^{xNH3}, and we compute the rate of clathrate dissociation required to equilibrate heat flux through the interface (R_{IO}). Then we determine the new upper and lower interface positions, R_{IO} and R_{OHP}, of the liquid water layer. Note that the methane dissociation temperature can be met only at the upper interface, R_{IO}. The methane outgassing rate is calculated from the clathrate dissociation rate assuming that all clathrate cages are filled with one methane molecule (1 kg of methane clathrate gives 134 g of gaseous methane); see above for a brief discussion of this assumption. Note that the methane outgassing rate during the last episode triggered by thermal convection within the outer layer is not computed in the same way. For the last episode, the clathrate dissociation is not controlled by the temperature at the upper interface of the ocean anymore, but by the temperature within hot icy plumes that penetrate the clathrate layer. We assume that the outgassing rate is proportional to surface heat flux and we display as figure 2 in the Letter itself an estimate of the outgassing rate assuming alternatively that 10% or 50% of the entire reservoir is outgassed. When the upper interface temperature,

T_{IO}, is between the methane dissociation temperature and the crystallization temperature of ammonia-water solution T_f^{xNH3}, and the outer layer is only made of clathrate, we compute the rate of cooling or warming of the ocean. Then we determine the new ocean temperature and the new lower interface position, R_{OHP}. When the upper interface, R_{IO}, reaches the crystallization temperature of ammonia-water solution T_f^{xNH3} (or the melting temperature of water ice), the cooling (or warming) rate of the ocean and the new interface positions, R_{IO} and R_{OHP}, are computed following the Grasset and Sotin scheme.

The values of gravity and pressure, the adiabatic temperature profile in the ocean, and the equilibrium temperature at each ice-ocean interface--all required to derive the thickening/thinning rate of both the outer layer and the high-pressure ice layer--are calculated by integrating the differential equations for mass, acceleration of gravity and pressure (e.g., Sohl *et al.* 2002). The surface radius of Titan, R_s, is not prescribed and is re-calculated at each time step in our evolution model, as the ice layers crystallize or melt. Only the global mass of silicate M_{sil}, water M_{H2O}, ammonia M_{NH3}, and methane M_{CH4} are prescribed in our model. The accurate calculation of the temperature evolution at the interface ocean-ice Ih is fundamental, considering the strong coupling between heat transfer and tidal dissipation via the temperature dependence of the ice Ih viscosity.

Figure 3 displays the interface position, R_{IO} and R_{OHP}, and temperature, T_{IO} and T_{OHP}, evolution as well as surface heat flux, Φ_{surf}, and eccentricity, e_{cc}, evolution for a typical simulation.

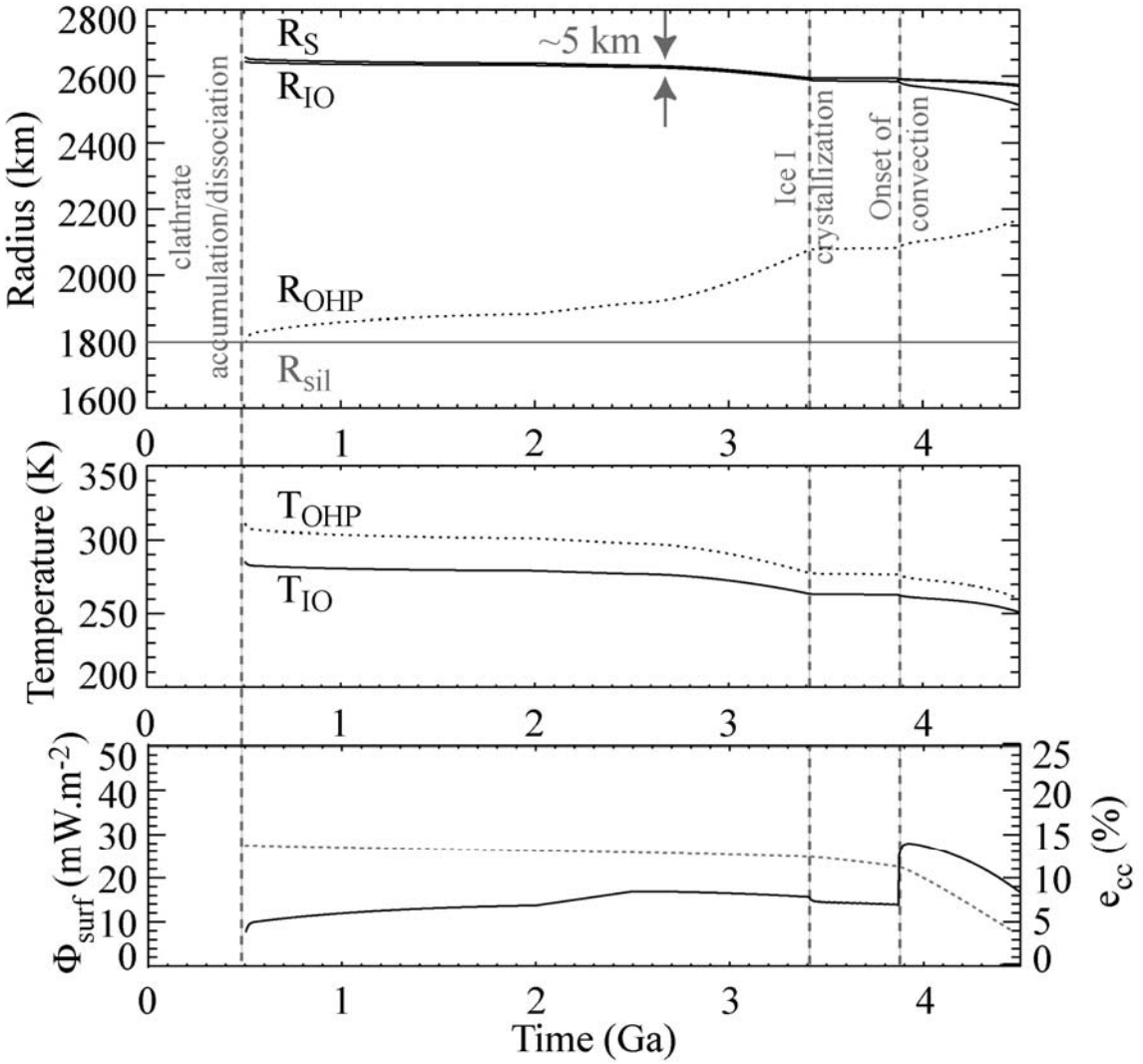

***Figure 3**: Surface radius R_s [solid line], and upper [solid line] and lower [dotted line] ocean interface radius, R_{IO} and R_{OHP} (upper graph), corresponding interface temperature, T_{IO} and T_{OHP} (middle graph), surface heat flux Φ_{surf} [solid line], and eccentricity e_{cc} [dotted line] (lower graph), as a function of time. In this simulation, we use scenario 2 for the evolution of the silicate core and we assume an ammonia fraction of 5% and a value of 10^{14} Pa.s for the viscosity of ice close to its melting point. Furthermore, the initial eccentricity is set to 13.5% in order to fit today's eccentricity value.*

Table 2: *Model parameters*

	Parameters	*Symbol*	*Unit*	*Value*	*Reference*
Orbit					
	Saturn's mass	M_S	kg	5.68×10^{26}	Sohl et al. 1995
	Initial eccentricity	E_0		[0.04-0.4]	*Free parameter*
	Current eccentricity	e_c		0.029	Sohl et al. 1995
	Current semimajor axis	a_c	km	1.2208×10^6	Sohl et al. 1995
	Current frequency	ω_c	rad.s-1	4.56×10^{-5}	Sohl et al. 1995
Internal structure					
	Titan's mass	M_T	kg	1.346×10^{23}	Sohl et al. 1995
	Mass of silicate	M_{sil}	kg	8.62×10^{22}	Sohl et al. 1995
	Mass of H_2O+NH_3	$M_{H2O-NH3}$	kg	4.84×10^{22}	Sohl et al. 1995
	Ammonia mass fraction (=$M_{NH3}/M_{H2O-NH3}$)	x_{NH3}	%	[0-8]	*Free parameter*
	Surface temperature	T_s	K	95	Sohl et al. 1995
	Surface pressure	P_s	Pa	1.5×10^5	Sohl et al. 1995
Interfaces	Surface	R_s	km	Computed	
	Ice I/ liquid	$R_{I/O}$	km	Computed	
	Liquid/HP ice	$R_{O/HP}$	km	Computed	
	HP ice/silicate	R_{sil}	km	1900	Sohl et al. 1995
Ice I	Density	ρ_I	$kg.m^{-3}$	920	Sotin et al. 1998
	S- and P- wave velocity	V_S/V_P	$m.s^{-1}$	1880/4000	Sotin et al. 1998
	Thermal conductivity	k_I	$W.m^{-1}.K^{-1}$		Kirk and Stevenson 1987
	$k_I(T)=k_1/T+k_2$	K_1/k_2		488/0.4685	
	Heat capacity	c_I	$J.kg^{-1}.K^{-1}$		Kirk and Stevenson 1987
	$cI(T)=c_1T+c_2$	C_1/c_2		7.037/185	
	Latent heat of fusion	L_I	$J.kg^{-1}$	284×10^3	Kirk and Stevenson 1987
	Thermal expansion	α_I	K^{-1}	$1.56 \times 10^{-4}(T/250)$	Kirk and Stevenson 1987
	Melting temperature				
	-of pure water ice	T_m^0	K	Computed	
	-in presence of ammonia	T_m^{NH3}	K	Computed	
	Newtonian viscosity	η_I	Pa.s	Eq. (1)	
	Viscosity at $T=T_m^0$	$\eta_{m,0}$	Pa.s	$[5.10^{13}$-$5.10^{14}]$	*Free parameter*
	Activation energy	E_a	$J.mol^{-1}$	50×10^3	Tobie et al. 2003
Methane clathrate	Density	ρ_{MH}	$kg.m^{-3}$	920	Loveday et al. 2001
	Thermal conductivity	k_{MH}	$W.m^{-1}.K^{-1}$	0.5	Sloan 1998
	Heat capacity	c_{MH}	$J.kg^{-1}.K^{-1}$	1600	Sloan 1998
	Latent heat of dissociation	L_{MH}	$J.kg^{-1}$	300×10^3	Sloan 1998
Liquid water	Density	ρ_w	$kg.m^{-3}$	1000	Tobie et al. 2003
	S- and P- wave velocity	V_S/V_P	$m.s^{-1}$	0/1500	Tobie et al. 2003
	Heat capacity	c_w	$J.kg^{-1}.K^{-1}$	4180	Kirk and Stevenson 1987
	Thermal expansion	a_w	K^{-1}	3×10^{-4}	Grasset et al. 2000
High pressure ice	Density	ρ_w	$kg.m^{-3}$	1310	Grasset et al. 2000
	S- and P- wave velocity	V_S/V_P	$m.s^{-1}$	1880/4000	Sotin et al. 1998
	Latent heat of fusion	L_{HP}	$J.kg^{-1}$	294×10^3	Kirk and Stevenson 1987
	Heat capacity	c_{HP}	$J.kg^{-1}.K^{-1}$	1925	Kirk and Stevenson 1987
Silicate	Density	ρ_{sil}	$kg.m^{-3}$	3000	Sohl et al. 1995
	S- and P- wave velocity	V_S/V_P	$m.s^{-1}$	4500/8000	Tobie et al. 2003
	Radiogenic heating	H_0	$W.kg^{-1}$	4×10^{-11}	Deschamps and Sotin 2001
	Decay constant	λ	s^{-1}	1.38×10^{-17}	Deschamps and Sotin 2001

REFERENCES:

Croft, S. K.; Lunine, J. I.; Kargel, J. Equation of state of ammonia-water liquid. *Icarus* 73, 279-293 (1988).

Deschamps, F., Sotin, C. Thermal convection in the outer shell of large icy satellites. *J. Geophys. Res.* 106(E3), 5107-5121 (2001).

Dickens, G. R.; Quinby-Hunt, M. S. Methane hydrate stability in pore water: A simple theoretical approach for geophysical applications *J. Geophys. Res*. 102(B1), 773-784 (1997).

Dyadin, Y. A., Aladko, E. Y. And Larionov, E. G. Decomposition of methane hydrates up to 15 kbar, *Mendeleev Comm.***,** 34-35 (1997).

Dumoulin, C., Doin, M.-P., Fleitout, L. Heat transport in stagnant lid convection with temperature- and pressure-dependent Newtonian or non-Newtonian rheology. *J. Geophys. Res.* 104(B6), 12759-12778 (1999).

Durham, W. B.; Kirby, S. H.; Stern, L. A.; Zhang, W. The strength and rheology of methane clathrate hydrate**.** *J. Geophys. Res.* 108(B4), pp. ECV 2-1, CiteID 2182, DOI 10.1029/2002JB001872 (2003).

Grasset, O., Sotin, C. The cooling rate of a liquid shell in Titan's interior. *Icarus* 123, 101-112 (1996).

Grasset, O.; Parmentier, E. M. Thermal convection in a volumetrically heated, infinite Prandtl number fluid with strongly temperature-dependent viscosity: Implications for planetary evolution. *J. Geophys. Res.* 103, 18171-18181 (1998).

Grasset O. & Pargamin, J. The ammonia water system at high pressures: implications for the methane of Titan. *Planet. Space Sci*. 53, 371-384 (2005).

Hemley, R. J., Jephcoat, A. P., Mao, H. K., Zha, C. S., Finger, L. W., Cox, D. E. Static compression of H2O-ice to 128 Gpa (128 Mbar). *Nature* 330, 737-740 (1987).

Karato, S.-I.; Wu, P. Rheology of the upper mantle: A synthesis. *Science* 260, 771-778 (1993).

Kirk, R. L.; Stevenson, D. J. Thermal evolution of a differentiated Ganymede and implications for surface features. *Icarus* 69, 91-134 (1987).

Klapproth, A., Goreshnik, E., Staykova, D. K., Klein, H., Kuhs, W. Structural studies of gas hydrates. *Can. J. Phys*. 81(1/2), 503-518 (2003).

Loveday, J. S., Nelmes, R. J., Guthrie, M., Belmonte, S. A., Allan, D. R., Klug, D. D., Tse, J. S., Handa, Y. P. Stable methane hydrate above 2 GPa and the source of Titan's atmospheric methane. *Nature* 410, 661-663 (2001).

Loveday, J. S., Nelmes, R. J. High-pressure neutron diffraction and models of Titan. *High Pressure Res.* 23, 41-47 (2003).

Lunine, J. I., Stevenson, D. J. Clathrate and ammonia hydrates at high pressure - Application to the origin of methane on Titan. *Icarus* 70, 61-77 (1987).

Peale, S. J. Origin and Evolution of the Natural Satellites. *Annual Rev. Astron. Astrophys.* 37, 533-602 (1999).

Sears, W. D. Tidal dissipation in oceans on Titan. *Icarus* 113, 39-56 (1995)

Schubert, G., Spohn, T. Thermal history of Mars and the sulfur content of its core**.** *J. Geophys. Res.* 95, 14095-14104 (1990).

Sloan E.D. Clathrates hydrates of natural gases. Marcel Dekker, Inc. New York 2nd edition (1998).

Sohl, F., Sears, W. D., Lorenz, R. D. Tidal dissipation on Titan. *Icarus* 115, 278-294 (1995).

Sohl, F., Spohn, T., Breuer, D., Nagel, K. Implications from Galileo observations on the interior structure and chemistry of the Galilean satellites. *Icarus* 157, 104-119 (2002).

Sohl, F., Hussmann, H., Schwentker, B., Spohn, T., Lorenz, R. D. Interior structure models and tidal Love numbers of Titan. *J. Geophys. Res.* 108(E12), pp. 4-1, CiteID 5130, DOI 10.1029/2003JE002044 (2003).

Sotin, C., Grasset, O., Beauchesne, S. 1998. Thermodynamical Properties of High Pressure Ices. Implications for the Dynamics and Internal Structure of Large Icy Satellites. In *Solar System Ices*, Based on reviews presented at the international symposium "Solar system ices" held in Toulouse, France, on March 27-30, 1995 Publisher: Dordrecht Kluwer Academic Publishers, Astrophysics and space science library (ASSL) Series vol no 227. ISBN0792349024., p.79.

Stengel, K. C., Oliver, D. C., Booker, J. R. Onset of convection in a variable viscosity fluid. *J. Fluid. Mech.* 120, 411-431 (1982).

Tobie, G. Impact of tidal heating on the geodynamical evolution of Europa and Titan. *PhD thesis*, University of Paris, France (2003).

Tobie, G., Choblet, G., Sotin, C. Tidally heated convection: Constraints on Europa's ice shell thickness. *J. Geophys. Res.* 108(E11), pp. 10-1, CiteID 5124, DOI 10.1029/2003JE002099 (2003).

Tobie, G., Grasset, O., Lunine, J. I., Mocquet, A., Sotin, C. Titan's internal structure inferred from a coupled thermal-orbital model. *Icarus* **175**, 496-502 (2005a).

Tobie, G., Mocquet, A., Sotin C. Tidal dissipation within large icy satellites: Applications to Europa and Titan. *Icarus*, 177, 534-549 (2005b).